

Intrinsic Two-Dimensional Ferroelectricity with Dipole LockingJun Xiao,¹ Hanyu Zhu,¹ Ying Wang,¹ Wei Feng,² Yunxia Hu,² Arvind Dasgupta,³ Yimo Han,⁴ Yuan Wang,¹ David A. Muller,^{4,5} Lane W. Martin,^{3,6} PingAn Hu,² and Xiang Zhang^{1,6,*}¹*NSF Nanoscale Science and Engineering Center (NSEC), University of California, Berkeley, California 94720, USA*²*School of Materials Science and Engineering, Harbin Institute of Technology, Harbin 150080, People's Republic of China*³*Department of Materials Science and Engineering, University of California, Berkeley, California 94720, USA*⁴*Department of Applied and Engineering Physics, Cornell University, Ithaca, New York 14853, USA*⁵*Kavli Institute at Cornell for Nanoscale Science, Ithaca, New York 14853, USA*⁶*Materials Sciences Division, Lawrence Berkeley National Laboratory, 1 Cyclotron Road, Berkeley, California 94720, USA* (Received 3 October 2017; revised manuscript received 10 April 2018; published 31 May 2018)

Out-of-plane ferroelectricity with a high transition temperature in ultrathin films is important for the exploration of new domain physics and scaling down of memory devices. However, depolarizing electrostatic fields and interfacial chemical bonds can destroy this long-range polar order at two-dimensional (2D) limit. Here we report the experimental discovery of the locking between out-of-plane dipoles and in-plane lattice asymmetry in atomically thin In_2Se_3 crystals, a new stabilization mechanism leading to our observation of intrinsic 2D out-of-plane ferroelectricity. Through second harmonic generation spectroscopy and piezoresponse force microscopy, we found switching of out-of-plane electric polarization requires a flip of nonlinear optical polarization that corresponds to the inversion of in-plane lattice orientation. The polar order shows a very high transition temperature (~ 700 K) without the assistance of extrinsic screening. This finding of intrinsic 2D ferroelectricity resulting from dipole locking opens up possibilities to explore 2D multiferroic physics and develop ultrahigh density memory devices.

DOI: [10.1103/PhysRevLett.120.227601](https://doi.org/10.1103/PhysRevLett.120.227601)

Ferroelectric ordering dictates electrically switchable macroscopic polarization, arising from spontaneous alignment of electric dipoles [1,2]. Such a collective phase reveals a fundamental interplay between crystal symmetry and quasiparticle interactions [3,4]. The development of ferroelectric materials such as barium titanate (BaTiO_3) was also prompted by applications like electromechanical actuators and storage devices [5]. However, the strength of polarization and transition temperature drop as ferroelectric films scale down due to the reduced long-range Coulomb coupling and enhanced depolarization field, and ferroelectricity disappears below a critical thickness around several to tens of nanometers [1,6–8]. In addition, interfacial bonding related strain and chemical environment can also deteriorate thin film ferroelectricity [9–11]. In contrast, the emerging van der Waals layered materials have strong intralayer chemical bonds but weak interlayer interactions, and thus could provide a pathway to eliminate the role of interfacial defects and strain. With the presence of this strong anisotropy, 2D layered materials may go beyond such limitations and are unique platforms to study fundamental electronic and structural ordering in two dimensions [12–14]. Furthermore, the ferroelectric switching allows the control of asymmetry-induced properties in 2D layered materials such as spin-orbit coupling, valley degree of freedom, and anisotropic transport [15,16].

Here we experimentally demonstrate intrinsic out-of-plane 2D ferroelectric ordering in atomically thin In_2Se_3 crystals with thickness down to 3 nm, and verify the unique polarization locking mechanism in accordance to the theoretical prediction [17]. Each In_2Se_3 layer contains five triangular atomic lattices stacked in the sequence of Se–In–Se–In–Se through covalent bonds and belongs to R3m space group (No. 160). The asymmetric position of the Se atom in the middle spontaneously breaks the centrosymmetry, providing two energetically degenerate states with opposite out-of-plane electric polarization and in-plane asymmetry with reverse second-order nonlinear polarization [Figs. 1(a) and 1(b)]. The stabilization of ferroelectricity is achieved primarily through the out-of-plane and in-plane polarization locking enforced by unique covalent bond configuration of In_2Se_3 crystal, instead of long-range Coulomb interaction in conventional ferroelectric materials [18]. To erase or even flip the out-of-plane electrical polarization, the middle Se atom must also move laterally (~ 100 pm), accompanied by the In–Se covalent bonds breaking and forming [17]. It is fundamentally distinct from traditional ferroelectric switching where small uniaxial atomic distortions (~ 10 pm) occur without bond breaking in perovskite oxides, or via molecular chain rotation in PVDF [19]. Such additional in-plane atomic movement enforced by structural locking provides strong resistance for out-of-plane polarization against the

depolarization field. Accordingly, the calculated domain wall energy is also several times to more than 1 order of magnitude larger than that in perovskite oxides such as PbTiO_3 and BaTiO_3 [17,20,21]. These features also distinguish the ferroelectricity in In_2Se_3 from recent reports on atomically thin SnTe and CuInP_2S_6 [22,23], whose polarization only involves either pure in-plane or out-of-plane atomic distortion without breaking of covalent bonds. As a consequence, SnTe cannot exhibit out-of-plane polar order, while the ferroelectricity in CuInP_2S_6 does not exist below 50 nm in the absence of extrinsic electronic screening by a conductive substrate.

We prepared atomically thin membranes of In_2Se_3 by both exfoliation and van der Waals epitaxial growth (Supplemental Material [24], Sec. I) [25,26]. Their thickness was then determined by atomic force microscopy, and the single layer step height is 1 nm (Supplemental Material [24], Sec. II and Fig. S1). To verify the presence of in-plane and out-of-plane asymmetry, which is the prerequisite for ferroelectricity, we performed SHG studies with normal and oblique incidence at ambient conditions (Supplemental Material [24], Secs. I and III, Fig. S2). First, the SHG signal from a trilayer sample on insulating mica substrate can be observed under normal incidence (Fig. S3a in Supplemental Material [24]), which indicates inversion symmetry breaking with the presence of in-plane nonlinear optical polarization. The polarization-resolved SHG shows a sixfold intensity pattern when the normal incident excitation and detection polarization are rotated collinearly [Fig. 1(c)]. Given the coordinate axes depicted in Fig. 1(a), the responsible tensor components for the SHG signal in Fig. 1(c) are χ_{xxx} , χ_{xyy} , χ_{yxy} , and χ_{yyx} according to the R3m space group. Based on detailed symmetry analysis (Supplemental Material [24], Sec. III) [27,28], the maximum of each lobe corresponds to the In—Se bond armchair direction. Although this threefold rotational symmetry prohibits in-plane electric dipole polarization, it gives an effective in-plane second-order optical dipole emission due to inversion symmetry breaking [29]. Next, we used angle-resolved polarization-selective SHG measurements to detect the out-of-plane dipole [30]. By rotating the crystal to make the In—Se bond direction perpendicular to both the incident and detecting polarization direction, the SHG induced by the in-plane dipole is made extinct. Then the vertical electric field in a tilted beam drives the out-of-plane dipole and gives rise to a SHG signal (Fig. S3b in Supplemental Material [24]). Figure 1(d) shows the incident angle dependent SHG from the out-of-plane dipole in the same trilayer sample, normalized with collection efficiency. As the tilt angle increases, SHG intensity increases as the z component of the optic electric field becomes stronger and is symmetric for positive and negative tilt angle. This observation confirmed the presence of an out-of-plane asymmetry in the In_2Se_3 ultrathin crystals, which is the prerequisite for 2D out-of-plane

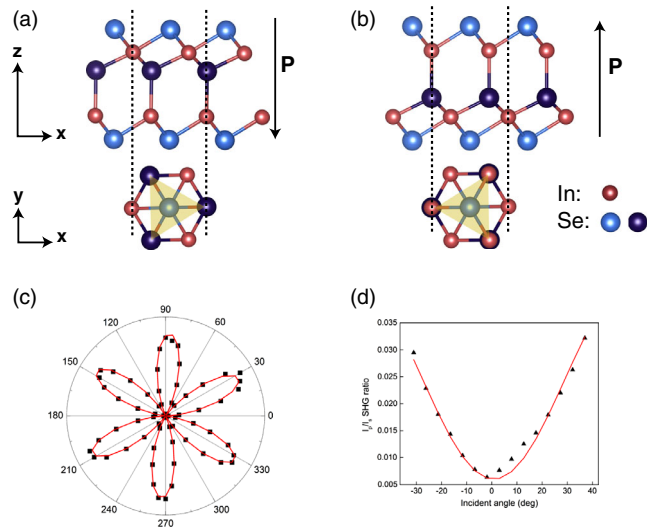


FIG. 1. Characterization of 2D In_2Se_3 . (a), (b) Side and top view of two energy-degenerate ferroelectric In_2Se_3 structures. Single quintuple layer consists of covalently bonded indium and selenium triangular lattices. The crystal belongs to R3m space group (No. 160). The polarization flipping requires locked out-of-plane and in-plane motion of middle Se atom (purple ball) accompanied by covalent bond breaking and formation, and reverses both the out-of-plane polarization and the in-plane lattice orientation with nonlinear optical polarization. (c) SHG polarization pattern of a trilayer triangular In_2Se_3 on mica substrate under normal incidence as a function of crystal angle. The threefold rotational symmetry manifests through the sixfold SHG intensity pattern (black square) when the polarization of the optical excitation and detection are rotated collinearly. Red curve shows the fitting by $I = I_0 \cos^2(3\theta + \theta_0)$, θ is crystal angle. (d) Out-of-plane dipole probed by angle resolved polarization-selective SHG on the same trilayer sample. Angle-dependent SHG intensity ratio I_p/I_s increases symmetrically with tilted incidence (black triangular) and agrees well with the model of response from out-of-plane dipole to vertical electrical oscillation field, indicating the ratio (13.6:1) between in-plane and out-of-plane second-order susceptibility at 1080 nm pump (red curve, see Supplemental Material [24], Sec. III for model details).

ferroelectricity. The ratio between in-plane and out-of-plane second-order susceptibility is 13.6:1 at the 1080 nm pump (Supplemental Material [24], Sec. III), consistent with the theoretical estimation that the static in-plane dipole is more than 1 order of magnitude larger than the out-of-plane dipole [17]. An annular dark-field scanning transmission electron microscopy (ADF-STEM) cross-section image of a multilayer In_2Se_3 also confirms the asymmetric ferroelectric crystal structure as predicted (Supplemental Material [24], Sec. IV and Fig. S4). Meanwhile, the samples with strong SHG signal display the same Raman characteristic peaks (Supplemental Material [24], Sec. and Fig. S5), as reported for α -phase In_2Se_3 [25].

In addition to the presence of dipoles, SHG and complementary PFM mapping of the trilayer at room temperature reveals domains and domain boundaries as

shown in Fig. 2. The region with stronger SHG displays larger piezoresponse, while the region with weaker SHG shows smaller piezoresponse amplitude. The correlation indicates that the as-grown sample contains domains with different net dipole strength. We verified that the dipole strength difference does not come from composition inhomogeneity, because both regions give the same Raman spectra (Fig. S6a in Supplemental Material [24]), meaning they have the same crystal phase. Therefore, we postulate that for the as-grown sample, some regions are well aligned along one polarization, while other regions may partially include lattice configuration with opposite polarization and reduce the average nonlinear optical response. Similar intensity variation has also been observed for SHG generated by out-of-plane dipole (Fig. S6b in Supplemental Material [24]). In addition, in the SHG image we observed dark lines within the area that has uniform optical contrast [Fig. 2(a)]. By superimposing these dark lines onto the piezoresponse and the phase mapping [blue curves in Figs. 2(b) and 2(c)], we found that they always occur at the boundaries of two 180-degree domains with comparable piezoresponse and SHG amplitude. The consistency proves that they result from destructive interference between the optical fields from adjacent domains with opposite polarizations (Supplemental Material [24], Sec. VII) [31]. On the other hand, for the boundary between a domain with large positive piezoresponse and a domain with small negative piezoresponse, SHG dark lines are

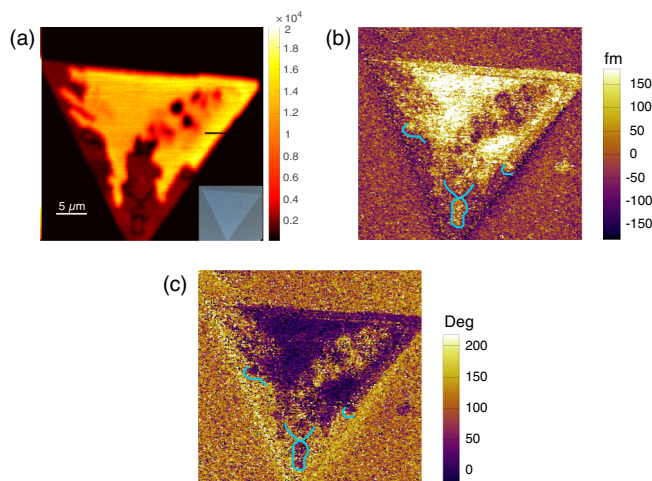


FIG. 2. Visualization of domain structure in 2D In_2Se_3 by SHG and piezoresponse mapping. (a) SHG mapping of the 3-nm In_2Se_3 crystal, showing intensity contrast in different regions corresponding to domains with different dipole strength that match well with the piezoresponse mapping in (b). The inset is the optical image of the same sample. SHG intensity dark lines are observed within the region of nearly uniform optical contrast and SHG intensity, that also match the boundaries between domains with 180° piezoresponse phase contrast in (c) (blue curves). They originate from the destructive interference from the oppositely polarized domains.

shadowed due to the imperfect optical destructive interference.

Beyond the presence of polar structures with opposite spontaneous polarizations, we also demonstrated the switch of the polarization by applying electric field. Indeed, for ultrathin ferroelectric In_2Se_3 , large out-of-plane field (~ 1 V/nm) is predicted to flip the out-of-plane polar order. In the following, we demonstrated such polarization switching with vertical electric bias at room temperature. The sample was prepared by transferring the as-grown In_2Se_3 flakes onto strontium ruthenium oxide (SrRuO_3) thin film deposited on a (001)-oriented strontium titanate (SrTiO_3) substrate, which served as the back electrode. The electric field was applied through a conductive tungsten carbide probe with radius of 20 nm, and then the polarization switching was observed separately through inverse piezoelectric effect by resonance-enhanced piezoresponse force microscopy (Supplemental Material [24], Sec. VIII). Figure 3(a) shows the single-point off-field hysteresis loop of the piezoresponse as a function of poling electric field for a trilayer flake. With small probe voltage of 0.5 V, the coercive field of this piezoresponse loop is about 2–3 V over the 3-nm thickness, comparable to the theoretical prediction. Such observed large coercivity confirms the large energy barrier between the two polarization states, which is necessary to combat the depolarization field at the 2D limit. As the probe voltage increases to 1.5 V close to the coercive field, the loop collapses in both amplitude and width. This is a clear signature of field-switchable electromechanical deformation expected from ferroelectricity in In_2Se_3 , and distinguished from the electrostatic force-induced artifacts from charging in non-ferroelectric materials [32]. Based on the obtained coercive field of 3-nm-thick the trilayer, we further observed areal ferroelectric domain reversal by scanning the probe with constant bias. Both positive and negative piezoresponse domains were written onto the trilayer sample as shown in Fig. 3(b). The pattern remained stable in ambient conditions for at least three days when it was probed again. It should be noted that although other contributions (e.g., injected charge, chemical changes, diffusion of species, etc.) can give rise to PFM contrast [33,34], the long-term stability of this signal suggests a link with the structural change and not one of these other spurious effects. In particular, we exclude the charging effect as the source of the electromechanical response, which should quickly dissipate for ultrathin semiconducting film on conductive substrate.

More strikingly, the unique polarization locking relationship in the In_2Se_3 crystal structure requires that the in-plane atomic motion be locked with the out-of-plane polarization switching, and enables control of in-plane asymmetry by out-of-plane electric fields. To demonstrate such control, we first selected one region of a trilayer In_2Se_3 sample on the $\text{SrRuO}_3/\text{SrTiO}_3$ (001) substrate showing strong SHG under normal incidence originating from in-plane dipoles

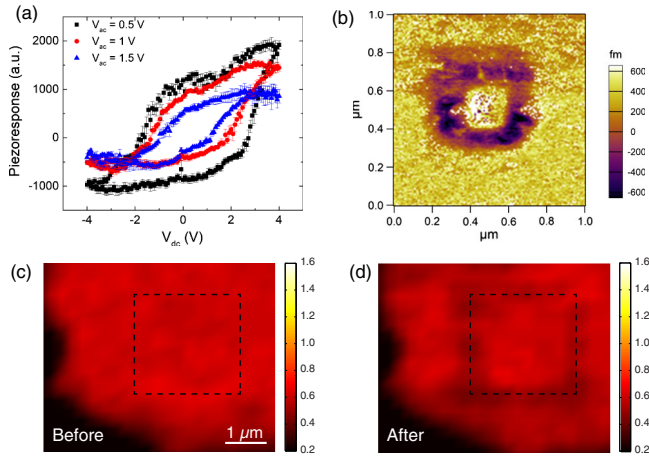


FIG. 3. Electrically switching the out-of-plane ferroelectric polarization and corresponding in-plane atomic configuration through dipole locking. (a) The hysteresis of remnant out-of-plane polarization of a 3-nm-thick In_2Se_3 crystal on conductive SrRuO_3 , as a function of perpendicular poling voltage. Black, red, blue curves represent the normalized piezoresponse measured with $V_{\text{ac}} = 0.5, 1, \text{ and } 1.5$ V, respectively. The collapse of the hysteresis loop agrees very well with the behavior of the conventional field-switchable ferroelectrics and is in contrast to the charging artifact of dielectrics. (b) Polarized domain patterned by electrically biased scanning probe and measured by PFM. The inner box corresponds to positive applied voltage (+6 V) and positive piezoresponse while the outer box to negative voltage (−6 V) and negative piezoresponse. (c) SHG intensity mapping on another trilayer In_2Se_3 sample before PFM reversed poling. The area enclosed by dashed line was then scanning by a negatively biased AFM tip. The color bar is in linear scale with arbitrary unit. (d) SHG mapping after the electrical reversed poling. It shows dark lines at the boundary of the patterned area resulting from destructive interference, which indicates the reversal of in-plane crystal orientation and corresponding non-linear optical polarization after reversed electrical poling.

[Fig. 3(c)]. Next, a square region was scanned by a negatively biased probe and enclosed by a dashed line [Fig. 3(c)]. The “writing” condition of negative electrical bias is the same as that applied in Fig. 3(b), where the domain flipping at a single point was achieved during the hysteresis loop measurement. After the writing process, the orientation of the in-plane dipole was probed by SHG under normal incidence. Compared with the mapping before patterning, it showed nearly uniform SHG intensity distribution outside the writing region as well as nearly uniform SHG intensity inside after reversal poling [Fig. 3(d)]. Notably, we also observed clear dark lines with low SHG intensity exactly overlapping with the boundaries defined by the PFM writing pattern, evidencing destructive optical interference because of the reversal of the in-plane nonlinear optical polarization and corresponding in-plane lattice asymmetry by the out-of-plane electric field patterning. Such observations further prove the strict locking between in-plane and out-of-plane dipoles and

allows electrical switching of in-plane crystalline symmetry by vertical electric field.

Finally, we observed evidence of a temperature-induced phase transition in the ultrathin In_2Se_3 around 700 K by temperature-dependent SHG (Fig. 4). Typically, increasing the temperature produces strong thermal fluctuations which act to destabilize the spontaneous polarization and drive the material into a high-temperature, high-symmetry structure possessing inversion symmetry. Similar effects were observed for a four-layer In_2Se_3 crystal transferred on a SiO_2/Si substrate. We first observed gradual SHG intensity decrease as a function of temperature over a broad range. The slow amplitude reduction of the SHG signal again confirms the robustness of the polar order. Starting at ~ 600 K, a sharp SHG intensity drop occurs, indicating the rapid disappearance of spontaneous polarization and the potential transition to a centrosymmetric phase. The observed high transition temperature is attributed to the energy difference between ferroelectric and high-temperature phases and the large kinetic transition barrier involving both in-plane and out-of-plane bond reconfiguration.

The realization of intrinsic out-of-plane ferroelectricity in ultrathin crystal is important for exploration on novel phase ordering with quantum confinement and enhanced quasiparticle interactions [35,36], which is absent in the thick films. Unconventional phase competition is expected when the depolarization field becomes significant in ultrathin film with a thickness of several nanometers. Also, the large mechanical and electrical tunability of atomically thin layered materials [37–39], may not only reveal rich phase transition physics but enable versatile ultrathin ferroelectric

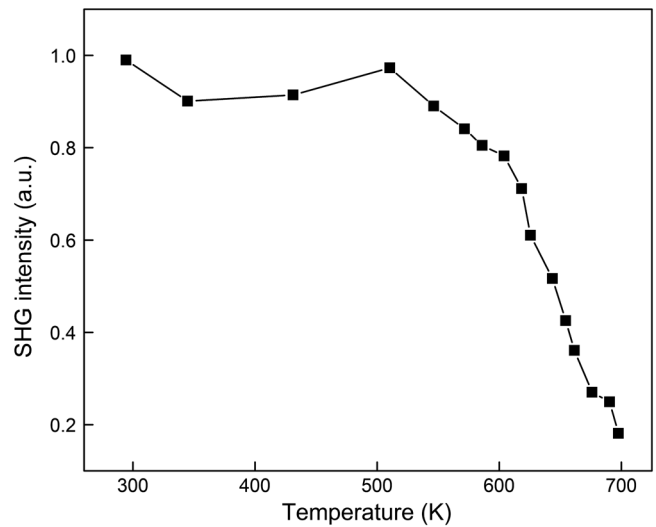


FIG. 4. Observation of temperature-dependent ferroelectric to centrosymmetric phase transition. The SHG intensity and the corresponding ferroelectric ordering remains robust as a four-layer In_2Se_3 sample on SiO_2/Si substrate was heated from room temperature to 600 K. It then dropped sharply to about one-sixth of the initial value when the temperature further increased to 700 K, indicating the disappearance of spontaneous polarization and the structural transition to a centrosymmetric phase.

devices. Although ferroelectricity in In_2Se_3 flakes with thickness of a few tens of nanometers was reported recently [35], it is far away from the atomically thin limit for exploration on above unique physics and applications. On the contrary, our study shows robust out-of-plane ferroelectricity in atomically thin In_2Se_3 (~ 3 nm) with an ultrahigh transition temperature (~ 700 K). Meanwhile, our first experimental confirmation of the strict locking between out-of-plane dipoles and in-plane covalent lattice asymmetry, a completely new mechanism to stabilize the 2D intrinsic ferroelectricity, provides a new degree of freedom to control structural and electronic ordering in layered materials and multiferroic heterostructures.

In conclusion, we demonstrated optical and electro-mechanical evidence in atomically thin In_2Se_3 crystal that satisfy the criteria for ferroelectric materials [1,40,41]: spontaneous polar ordering in the absence of an external electric field; switching of such polarization by an electric field. Such ferroelectricity is intrinsically stable against the depolarization field even on dielectric substrates with little screening, protected by dipole locking due to its unique covalent bond configuration. Furthermore, the ferroelectric phase of In_2Se_3 has high transition temperature ~ 700 K. This discovery features a new polarization switching mechanism involving covalent bond reconstruction and provides a unique platform to explore 2D ferroelectric physics and establish novel 2D optoelectronic devices based on the polarization locking relationship.

We acknowledge technical support from Ed Wong on high- T vacuum chamber preparation. J. X., H. Z., Y. W., Y. W., and X. Z. acknowledge the support from National Science Foundation (EFMA-1542741) and the King Abdullah University of Science and Technology (KAUST) Office of Sponsored Research (OSR) under Award No. OSR-2016-CRG5-2996. W. F., Y. H., and P. H. were supported by the National Natural Science Foundation of China (NSFC, No. 61390502 and No. 61505033). A. D. acknowledges support from the National Science Foundation under Grant No. DMR-1708615. L. W. M. acknowledges support from the Army Research Office under Grant No. W911NF-14-1-0104. Y. H. and D. A. M. were supported by the Cornell Center for Materials Research with funding from the NSF MRSEC program (DMR-1719875).

J. X., H. Z., and Y. W. contributed equally to this work.

*Corresponding author.
xiang@berkeley.edu

- [1] M. E. Lines and A. M. Glass, *Principles and Applications of Ferroelectrics and Related Materials* (Oxford University Press, New York, 2001).
[2] M. Dawber, K. M. Rabe, and J. F. Scott, *Rev. Mod. Phys.* **77**, 1083 (2005).

- [3] T. Egami, S. Ishihara, and M. Tachiki, *Science* **261**, 1307 (1993).
[4] A. K. Yadav, C. T. Nelson, S. L. Hsu, Z. Hong, J. D. Clarkson, C. M. Schlepüetz, A. R. Damodaran, P. Shafer, E. Arenholz, L. R. Dedon, D. Chen, A. Vishwanath, A. M. Minor, L. Q. Chen, J. F. Scott, L. W. Martin, and R. Ramesh, *Nature (London)* **530**, 198 (2016).
[5] J. F. Scott, *Science* **315**, 954 (2007).
[6] E. A. Eliseev, S. V. Kalinin, and A. N. Morozovska, *J. Appl. Phys.* **117**, 034102 (2015).
[7] C. H. Ahn, K. M. Rabe, and J.-M. Triscone, *Science* **303**, 488 (2004).
[8] J. Junquera and P. Ghosez, *Nature (London)* **422**, 506 (2003).
[9] Y. Wang, M. K. Niranjana, K. Janicka, J. P. Velez, M. Y. Zhuravlev, S. S. Jaswal, and E. Y. Tsymlal, *Phys. Rev. B* **82**, 094114 (2010).
[10] C. G. Duan, R. F. Sabirianov, W. N. Mei, S. S. Jaswal, and E. Y. Tsymlal, *Nano Lett.* **6**, 483 (2006).
[11] C.-L. Jia, V. Nagarajan, J.-Q. He, L. Houben, T. Zhao, R. Ramesh, K. Urban, and R. Waser, *Nat. Mater.* **6**, 64 (2007).
[12] X. Xi, Z. Wang, W. Zhao, J.-H. Park, K. T. Law, H. Berger, L. Forró, J. Shan, and K. F. Mak, *Nat. Phys.* **12**, 139 (2016).
[13] Y. Saito, Y. Kasahara, J. Ye, Y. Iwasa, and T. Nojima, *Science* **350**, 409 (2015).
[14] Y. Yu, F. Yang, X. F. Lu, Y. J. Yan, H. ChoYong, L. Ma, X. Niu, S. Kim, Y.-W. Son, D. Feng, S. Li, S.-W. Cheong, X. H. Chen, and Y. Zhang, *Nat. Nanotechnol.* **10**, 270 (2015).
[15] K. F. Mak, K. He, J. Shan, and T. F. Heinz, *Nat. Nanotechnol.* **7**, 494 (2012).
[16] F. Xia, H. Wang, and Y. Jia, *Nat. Commun.* **5**, 4458 (2014).
[17] W. Ding, J. Zhu, Z. Wang, Y. Gao, D. Xiao, Y. Gu, Z. Zhang, and W. Zhu, *Nat. Commun.* **8**, 14956 (2017).
[18] G. A. Samara, T. Sakudo, and K. Yoshimitsu, *Phys. Rev. Lett.* **35**, 1767 (1975).
[19] W. J. Hu, D.-M. Juo, L. You, J. Wang, Y.-C. Chen, Y.-H. Chu, and T. Wu, *Sci. Rep.* **4**, 4772 (2014).
[20] M. Li, Y. Gu, Y. Wang, L. Q. Chen, and W. Duan, *Phys. Rev. B* **90**, 054106 (2014).
[21] B. Meyer and D. Vanderbilt, *Phys. Rev. B* **65**, 104111 (2002).
[22] K. Chang, L. Junwei, L. Haicheng, N. Wang, K. Zhao, A. Zhang, F. Jin, Y. Zhong, X. Hu, W. Duan, Q. Zhang, L. Fu, Q.-K. Xue, X. Chen, and S.-H. Ji, *Science* **353**, 274 (2016).
[23] F. Liu, L. You, K. L. Seyler, X. Li, P. Yu, J. Lin, X. Wang, J. Zhou, H. Wang, H. He, S. T. Pantelides, W. Zhou, P. Sharma, X. Xu, P. M. Ajayan, J. Wang, and Z. Liu, *Nat. Commun.* **7**, 12357 (2016).
[24] See Supplemental Material at <http://link.aps.org/supplemental/10.1103/PhysRevLett.120.227601> for experimental details on methods, angle dependent polarization resolved SHG analysis, In_2Se_3 crystal cross-section STEM and optical and PFM signal analysis related with domain structure and dipole locking.
[25] X. Tao and Y. Gu, *Nano Lett.* **13**, 3501 (2013).
[26] W. Feng, W. Zheng, F. Gao, X. Chen, G. Liu, T. Hasan, W. Cao, and P. Hu, *Chem. Mater.* **28**, 4278 (2016).
[27] L. M. Malard, T. V. Alencar, A. P. M. Barboza, K. F. Mak, and A. M. De Paula, *Phys. Rev. B* **87**, 201401 (2013).

- [28] Y. R. Shen, *Principles of Nonlinear Optics* (John Wiley & Sons, Inc., New York, 2002).
- [29] Y. Li, Y. Rao, K. F. Mak, Y. You, S. Wang, C. R. Dean, and T. F. Heinz, *Nano Lett.* **13**, 3329 (2013).
- [30] A.-Y. Lu, H. Zhu, J. Xiao, C.-P. Chuu, Y. Han, M.-H. Chiu, C.-C. Cheng, C.-W. Yang, K.-H. Wei, Y. Yang, Y. Wang, D. Sokaras, D. Nordlund, P. Yang, D. A. Muller, M.-Y. Chou, X. Zhang, and L.-J. Li, *Nat. Nanotechnol.* **12**, 744 (2017).
- [31] S. A. Denev, T. T. A. Lummen, E. Barnes, A. Kumar, and V. Gopalan, *J. Am. Ceram. Soc.* **94**, 2699 (2011).
- [32] N. Balke, P. Maksymovych, S. Jesse, A. Herklotz, A. Tselev, C. B. Eom, I. I. Kravchenko, P. Yu, and S. V. Kalinin, *ACS Nano* **9**, 6484 (2015).
- [33] S. Hong, J. Woo, H. Shin, J. U. Jeon, Y. E. Pak, E. L. Colla, N. Setter, E. Kim, and K. No, *J. Appl. Phys.* **89**, 1377 (2001).
- [34] N. Balke, S. Jesse, Q. Li, P. Maksymovych, M. B. Okatan, E. Strelcov, A. Tselev, and S. V. Kalinin, *J. Appl. Phys.* **118**, 072013 (2015).
- [35] Z. Ye, T. Cao, K. O'Brien, H. Zhu, X. Yin, Y. Wang, S. G. Louie, and X. Zhang, *Nature (London)* **513**, 214 (2014).
- [36] A. Chernikov, T. C. Berkelbach, H. M. Hill, A. Rigosi, Y. Li, O. B. Aslan, D. R. Reichman, M. S. Hybertsen, and T. F. Heinz, *Phys. Rev. Lett.* **113**, 076802 (2014).
- [37] K. F. Mak, K. He, C. Lee, G. H. Lee, J. Hone, T. F. Heinz, and J. Shan, *Nat. Mater.* **12**, 207 (2013).
- [38] J. T. Ye, Y. J. Zhang, R. Akashi, M. S. Bahramy, R. Arita, and Y. Iwasa, *Science* **338**, 1193 (2012).
- [39] D. Akinwande, N. Petrone, and J. Hone, *Nat. Commun.* **5**, 5678 (2014).
- [40] K. M. Rabe, C. H. Ahn, J. M. -M. Triscone, M. Dawber, and C. Lichtensteiger, *Physics of Ferroelectrics* (Springer, New York, 2007).
- [41] C. Kittel, *Introduction to Solid State Physics* (John Wiley & Sons, Inc., New York, 2004).